Asia-Pacific Journal of Science and Technology: Volume: 29. Issue: 05. Article ID.: APST-29-05-15. Research Article

APST

Asia-Pacific Journal of Science and Technology

https://www.tci-thaijo.org/index.php/APST/index

Published by Research Department,
Khon Kaen University, Thailand

Multi-Temporal InSAR analysis for monitoring the ground deformation of Mount Sinabung

Muhammad Hanif[1], Sarun Apichontrakul[1,*], Pakhrur Razi[2]

[1] Geoinformatics, Department of Computer Science, College of Computing, Khon Kaen University, Thailand
[2] Center of Disaster Monitoring and Earth Observation, Universitas Negeri Padang, Indonesia
[*]Corresponding author: sarunap@kku.ac.th

Received 15 October 2023
Revised 15 January 2024
Accepted 31 January 2024

Abstract

Deformation of a volcano's surface is a geohazard caused by volcanic activities and seismicity. Monitoring the deformations serves as a part of an early warning system that can mitigate disasters. Between 2017-2022, Mount Sinabung volcano's ground deformation was monitored and analyzed using Multi-Temporal Interferometry Synthetic Aperture Radar (InSAR) and spatial statistics. The results showed substantial changes in surface elevation. The maximum monthly inflation was 4.7 cm in 2020, while the maximum monthly deflation was -4.7 cm in 2018. The correlation between the number of monthly eruptions and deformation patterns was very weak at 0.09 to -0.09, which indicated that the volcano's eruptions did not lead to ground deformation around Mount Sinabung and vice versa. Moreover, the ground deformation at Mount Sinabung did not indicate a consistent or periodic pattern. Some areas experienced higher deformation rates than others, depending on the land cover and underground magmatic activities. The volcano surface has been inflating over the past six years with an average rate of 0.14 cm/year. Data from sample observation points recorded the highest rate of 1.74 cm/year at the mid-slope, and the lowest rate of 0.62 cm/year at the foot of the mountain. The mountain caldera showed a ground surface inflation rate of 1.53 cm/year. The data showed that, despite the absence of an explosive or magmatic eruption since Mount Sinabung returned to activity, its caldera and surface continue to undergo deformations at higher velocities. Future explosive eruptions are expected, and preemptive preparations for potential disasters should be planned.

Keywords: deformation, geohazard, InSAR, Sinabung, spatial statistics, volcano

1. Introduction

A geohazard is a natural disaster that is caused by geological or geophysical factors, which are often unavoidable. A volcanic eruption is one example that can be generally found along the Asia-Pacific Ring of Fire. The most recent volcanic eruption on the Sumatra island was from Mount Sinabung, which is one of the most active volcanoes in Indonesia. Mount Sinabung, which is situated in the northern portion of Sumatra Island, is a small stratovolcano, which is less than 5 km in diameter and has an elevation of 2,460 m [1]. After a 400-year-long dormant period, this volcano returned to activity with a phreatic eruption on August 27, 2010 [2]. The eruptive flows of lava and dense pyroclastic deposits were localized beneath each other due to deposits from the Toba caldera. Minor fumarolic activity was severely restricted to one of three small summit craters before the phreatic eruptions began in 2010, which marked the new beginning of Mount Sinabung's activity. This phenomenon proved that this mountain cannot be considered as completely extinct, and its activity continues to be observed today [3].

This volcanic geohazard has caused ecological, social, and economic losses, and has significantly impacted the morphology of the mountain. Eruptions from Mount Sinabung have destroyed agricultural areas at the foot of the mountain. Villagers and settlements have had to be relocated because of the volcanic deposits from the eruptions. These eruptions have also caused the deformation of the volcano [4]. The movement and existence of

active magma reservoirs in underground burrows has caused surface deformation; subsidence (or deflation), and uplift (or inflation) [3]. The impact of volcanic deformation is the creation of areas that are prone to deformation. Those areas, which have experienced deformation, will be more susceptible to future deformation. The deformed surface of the slopes around the volcano make it more prone to landslides, which can trigger a massive eruption. Geohazards, such as volcanic eruptions and deformations are usually unpredictable. Therefore, initial information like mountain surface deformation must constantly be observed in order to mitigate volcanic disasters [5]. Monitoring volcano deformation is vital for predicting volcanic activities and for developing efforts toward creating an early warning system for volcanic disasters. Information about volcanic deformation can also provide clues about the states and behaviors of magma, hydrothermal fluids, and gases that lie beneath the shallow surface

Advanced technologies, such as Interferometric Synthetic Aperture Radar (InSAR) and Global Navigation Satellite System (GNSS), have been widely applied in studies of urban land subsidence, landslides, tectonic deformation, and volcanic activities. Previous researchers have utilized this technology, yielding promising analysis results and demonstrating high-accuracy performance [6]. the Advanced Land Observing Satellite (ALOS-2) Phased Array type L-band Synthetic Aperture Radar (PALSAR) and Sentinel 1 can be used to monitor deformations of the entire areas of volcanoes and can serve as alternatives to relying on observation stations with limited measurement coverage [1,7]. It has contributed to policy recommendations for disaster mitigation [8] and has also played a pivotal role in monitoring dormant volcanoes to avert potential disasters. This information is indispensable for gaining insights into regular volcanic behavior and forms an integral component of endeavors to mitigate the risk of future volcanic eruptions [3]. Many studies have used InSAR data to monitor Mount Sinabung. Seipuloh et al. [8] and Lee et al. [9] studied the deformation of Mount Sinabung using ALOS/PALSAR images from 2007 to 2011, but the dataset was not periodic. Aditya A. [10] observed the deformation of Mount Sinabung with ALOS/PALSAR from 2014 to 2017. Razi et al. [11], used Sentinel 1 to study the deformation of Mount Sinabung before and after its volcanic eruption in 2018. However, with the limited data, they found no surface deformation trends or patterns around the volcano.

Most research studies that have used Sentinel-1 to study Mount Sinabung have only analyzed the surface deformation after eruption events. However, since 2010, eruptions of the volcano have become unpredictable, and its volcanic activity is still very aggressive. This has altered the physiography of the area irrespective of the number of eruptions. This study aimed to analyze the monthly data from Sentinel-1 from 2017 to 2022 using the Multi-Temporal InSAR analysis method in order to create a time series map of ground deformation around Mount Sinabung and to assess the correlation between the deformation patterns and the previous eruptions in the past 6 years.

2. Materials and methods

2.1 The studied area

Mount Sinabung is located in three sub-districts of Karo Regency (Tiganderket, Namanteran, and Payung) in North Sumatra Province in Indonesia. This mountain is a stratovolcano situated in the Semangko fault area and was formed from the Toba Tua Basin area, which is a remnant of Mount Toba system [2,7]. Several tectonic faults surround this mountain; the strike-slip ends at the foot of Mount Sinabung, and the second-order fault stretches from the northern region of Mount Sinabung to the Mount Sibayak area. Figure 1 shows the location and types of land cover of Mount Sinabung and its land cover map.

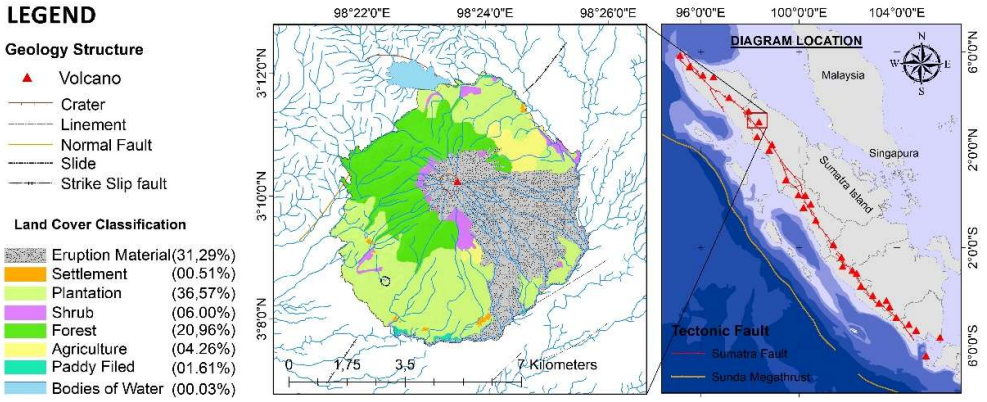

Figure 1 The studied area of Mount Sinabung in Karo Regency in Northern Sumatra in Indonesia.

2.2 Materials

This research used Sentinel-1 A satellite imagery, which was generated from synthetic-aperture radar (SAR) technology, and which relies on actively transmitting and receiving electromagnetic waves sequentially. The collected Sentinel-1 A dataset is a C-band radar image with wavelength of 5.5 cm. The dataset consisted of Level-1 Single Look Complex (SLC) with a ground range based on the Earth ellipsoid model WGS84, an incidence angle range between 18.3°-46.8° descending orbit with polarization VV-VH, and a beam interferometric wide swath of 250 km. This analysis utilized 72 months of data collected between 2017 and 2022. The Shuttle Radar Topography Mission (SRTM) data was obtained from the United States Geological Survey (USGS) for the co-registration process. The supporting spatial data, such as the administrative boundary and the land cover map, were obtained from the Indonesian Geospatial Information Agency (BIG). Records of Mount Sinabung's eruptions were obtained from legal data that had been published on the Magma Indonesia website [https://magma.esdm.go.id/]. This data was used to analyze the correlation between the eruption events and the deformation patterns. Table 1 shows the detailed records of the mountain's eruption events.

Table 1 A Record of the Volcanic Eruptions

No.	Month	Year	Eruptions	No.	Month	Year	Eruptions
1	January	2017	3	17	May	2018	3
2	February	2017	100	18	June	2018	1
3	March	2017	36	19	July	2018	1
4	April	2017	47	20	May	2019	7
5	May	2017	51	21	June	2019	1
6	June	2017	75	22	August	2020	22
7	July	2017	66	23	September	2020	1
8	August	2017	113	24	November	2020	8
9	September	2017	23	25	December	2020	4
10	October	2017	40	26	January	2021	8
11	November	2017	17	27	March	2021	22
12	December	2017	108	28	April	2021	30
13	January	2018	79	29	May	2021	11
14	February	2018	12	30	June	2021	2
15	March	2018	2	31	July	2021	4
16	April	2018	6				

Sources: Magma pusat vulkanologi dan mitigasi bencana geologi, 2023.

2.3 Methods

2.3.1 Differential Interferometry Synthetic Aperture Radar (DInSAR)

The DInSAR technique can detect volcanism activity, ground movements, and land subsidence, with outstanding results. This technique measures the relative motion based on two phases of two satellite images from different months to determine the deformation changes that had occurred [6,8]. The result of this analysis was the creation of a ground deformation map between 2017-2022. The DInSAR process is composed of the pre-processing steps (interferogram formation, net topographic effects, filtering, and multi-search), the data unwarping process, and the displacement analysis process. [10,11]. The technique exploits two phases of interferometry, which contain information that is related to topographical profiles, differences in orbital paths, coherence, deformations, and phase noise. Kim [12] noted that the coherence value is on a scale that ranges from 0 to 1, in which '0' indicates no relationship between the two images and '1' indicates a perfect correlation between them. The coherence threshold used in this research was based on a study by Ullo et. al. [13], in which a coherence value > 0.35 is considered indicative of good coherence for generating interferometric displacement values that are suitable for further analysis [14]. The initial output of interferometry is the phase value (ranging from 0 to 2), which is then converted into displacement (measured in meters) [10]. When processing the InSAR data, the phase unwrapping (PU) stage is a very crucial stage of the work in order to obtain the absolute phase value [9]. Phase absolute interferometric data was able to be obtained in the form of a displacement in meter units.

2.3.1 Spatial statistic analysis

Spatial statistics is a specialized branch of statistics that deals with geospatial data [15]. Spatial statistics primarily involves the application of statistical methods and analytical techniques that are utilized to unveil patterns, relationships, and variations that are present in the spatial data [16]. This research calculated the various descriptive statistics of the DInSAR data to examine changes in the reference pixels. The raster pixels used in this study were 15 cm^2. In this research, the calculated spatial statistics included the maximum, minimum, average, variance, and the standard deviation of the monthly deformation. The correlations between the ground deformation statistics and the number of eruptions each month were also analyzed. In this stage, the input data consisted of the

monthly deformation data for the entire mountain area as the independent variable (x) and the counts of monthly eruptions as the dependent variable (y). The analysis encompassed the entire area of the volcano.

3. Results and discussion

3.1 Time series coherence InSAR

The monthly ground deformation of Mount Sinabung was determined by utilizing InSAR analysis, which calculated the phase coherence and displacement values. The coherence value was selected as a reference for monthly coherence, and subsequently, the average coherence values of each research year were extracted, as shown in Figure 2, depicting the distribution of annual coherence values over the observation period. The most reliable average coherence value information from the InSAR analysis results for each year is provided in this figure. It is evident from the figure that in 2019, the coherence value ranged from 0.41 to 0.80; in 2020, it ranged from 0.32 to 0.91; and in 2021, it ranged from 0.37 to 0.88. Moreover, the average coherence value, which was determined in 2022, fell within the range of approximately 0.39 to 0.91. All these average coherence values can serve as valuable references for interferometric analysis since they surpassed the pre-defined threshold. The results of coherence extraction revealed that in 2017, there was an area with an average coherence >0.35, which covered 13% of the area. In 2018, the area exhibiting good coherence expanded to 25.1%, while in 2019, the region with selected coherence encompassed 14.5%. In 2020, an area of 15.8% exhibited this characteristic, while for 2021, it was only 13.7%. Finally, in 2022, the total observed mountain area with the highest coherence value was measured at 18.03%.

According to the land cover map in Figure 1, the majority of Mount Sinabung's terrain is covered by vegetation. Bare land and former eruptive material cover 31.2% of the area, and this is the only area that is potentially capable of producing high coherence values without interference from surface objects. Vegetative land cover almost always has low coherence. The existing land cover conditions represent one of the contributing factors that limits the extent of Mount Sinabung's surface area and can yield high coherence values in any interferogram analysis. It is important to acknowledge here that we cannot anticipate achieving an entirely perfect result across the entirety of the SAR image recordings of the mountain's surface. Romero [17] stated that a low coherence value in an observation area can be attributed to various factors, such as atmospheric conditions, vegetation, humidity changes, and types of land cover [16,18]. Even in light of the identified limitations stemming from the geographical conditions of the research subject, the outcomes of these observations can still serve as valuable references for analysis.

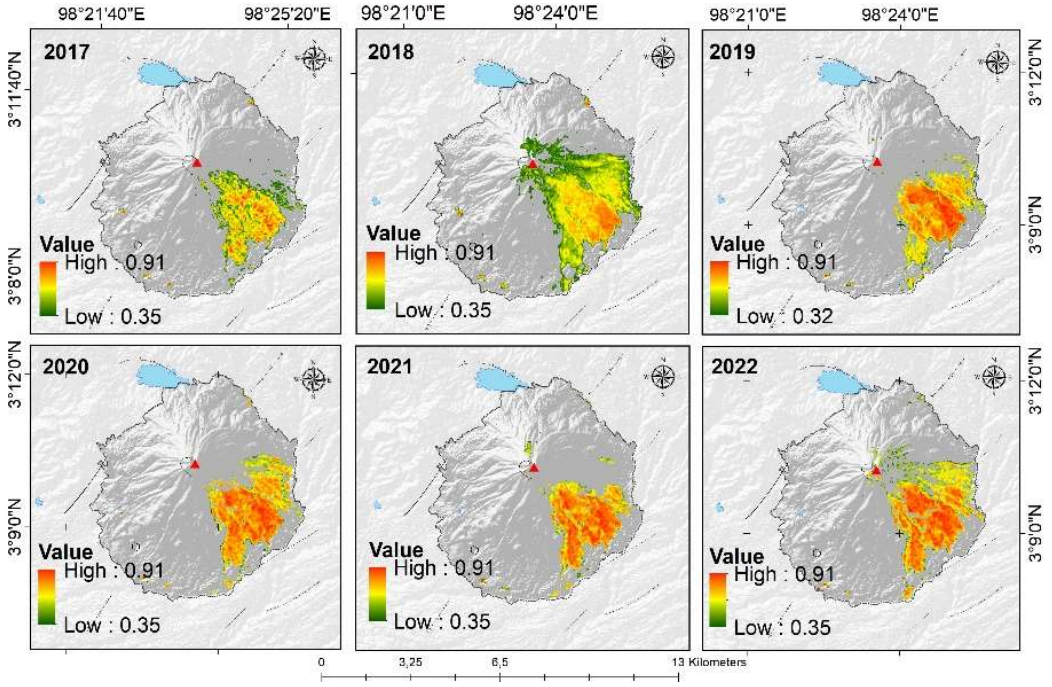

Figure 2 The average annual InSAR coherence (> 0.35) for each year from 2017 to 2022.

3.2 Monthly vertical deformation InSAR

The monthly vertical deformation of Mount Sinabung during the six years of observation (from 2017 to 2022) was successfully mapped through interferometric analysis (Figures 3a and 3b). The map legend denotes that the colors closer to red represent a maximum surface deflation of -4.7 cm, while those colors closer to blue signify a maximum surface inflation of 4.7 cm. The time-series maps provide insights into the historical distribution of inflation and deflation of the surface across the entire mountain. It is evident that the southeastern side of the mountain has experienced significant deformation fluctuations during each month of observation.

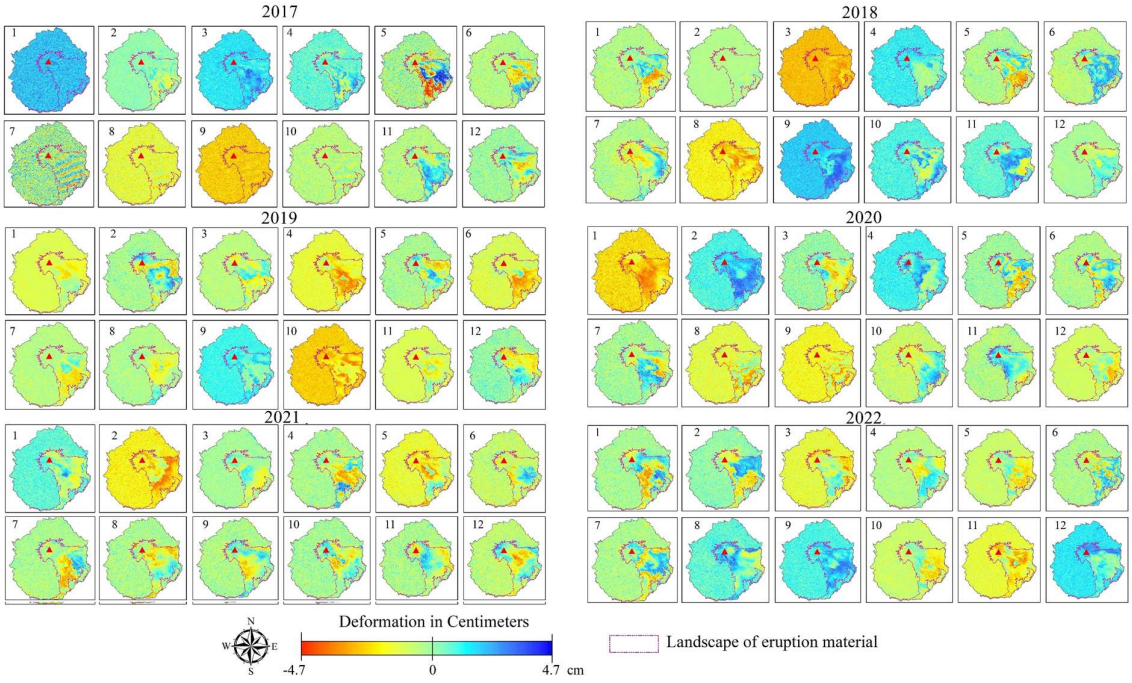

Figure 3 The monthly volcano ground deformation form January 2017 to December 2022.

There have been various instances of the volcano's ide rising and subsiding, as well as changes in surface elevation at different rates and patterns. This deformation data indicated that volcanic deformation is not a uniform natural occurrence across the volcano's surface. Nevertheless, the deformation of Mount Sinabung represents a continuous natural phenomenon that took place throughout the research period, affirming the presence of dynamic processes within the volcanic system.

The spatial distribution of deformation revealed that inflation had occurred in certain zones around the volcano while deflation had occurred in others. Figure 3 provide a comparison of the monthly deformations. It is important to note that the spatial distribution had been consistently concentrated in areas with previous eruptive material and open land spaces. However, the locations of maximum inflation and deflation points consistently underwent changes in their spatial distribution patterns. This dynamic zone also corresponded to an area with a coherence value exceeding a pre-determined threshold, which enabled more detailed observations to be conducted.

The spatial pattern analysis revealed that during specific periods, consisting of January and March of 2017, September of 2018, February of 2020, and September and December of 2022, a noticeable increase in deformation occurred across the majority of the areas. This increase is visually represented by a predominant blue coloration in these regions.

3.3 *The spatial statistics report*

Spatial statistical analysis was employed to assess the trends and characteristics of Mount Sinabung's deformation using multi-temporal data. This research calculated the ground deformation's maximum inflation and deflation values on a monthly basis, the average annual deformation, the standard deviation, and the variance from high coherence sample points around Mount Sinabung. The results, which are are presented in Table 2 and in Figures 4 and 5, reveal that there had been crucial ground deformation patterns at Mount Sinabung, which were determined to be erratic. In particular, there was the fact that the inflation patterns had not followed a consistent interval with regard to the historical deformation trend of the previous six years. These fluctuations, which had

been highly intricate and had occurred periodically, displayed substantial disparities in the magnitude of the displacement between surface inflation and deflation, as well as variations in spatial distribution. This data underscores the persistence of the deformation process even in the absence of volcanic eruptions.

Table 2 The annual spatial statistics of volcano deformation.

No.	Deformation Statistics from Sentinel 1 DInSAR (cm)			Sta-dev	Var
	Max-Inflation	Max-Deflation	Average		
2017	3.8	-3.7	-0.020	0.19	0.040
2018	3.8	-4.7	0.007	0.23	1.056
2019	2.1	-2.9	-0.020	0.23	0.056
2020	4.7	-2.1	0.240	0.23	0.056
2021	3.8	-1.1	0.43	0.22	0.054
2022	3.9	-3.9	0.220	1.43	0.050

Table 2 presents the variations in maximum deformation values for each year. In 2020, the highest maximum deformation value reached 4.7 cm, and the maximum deflation reached -4.70 cm. In contrast, in the year 2019, the lowest maximum inflation value of 2.1 cm was displayed, as well as the maximum deflation value of -2.9 cm. For both 2017 and 2022, the maximum inflation fell within the range of 3.8 to 3.9 cm, while the maximum deflation ranged from -3.7 to -3.9 cm. Meanwhile, the highest standard deviation value was found in 2022, with a value of 1.43 cm. Subsequently, the overall statical analyses of all the data were conducted to determine the deformation trends over the course of the six-year period, as depicted in Figure 4.

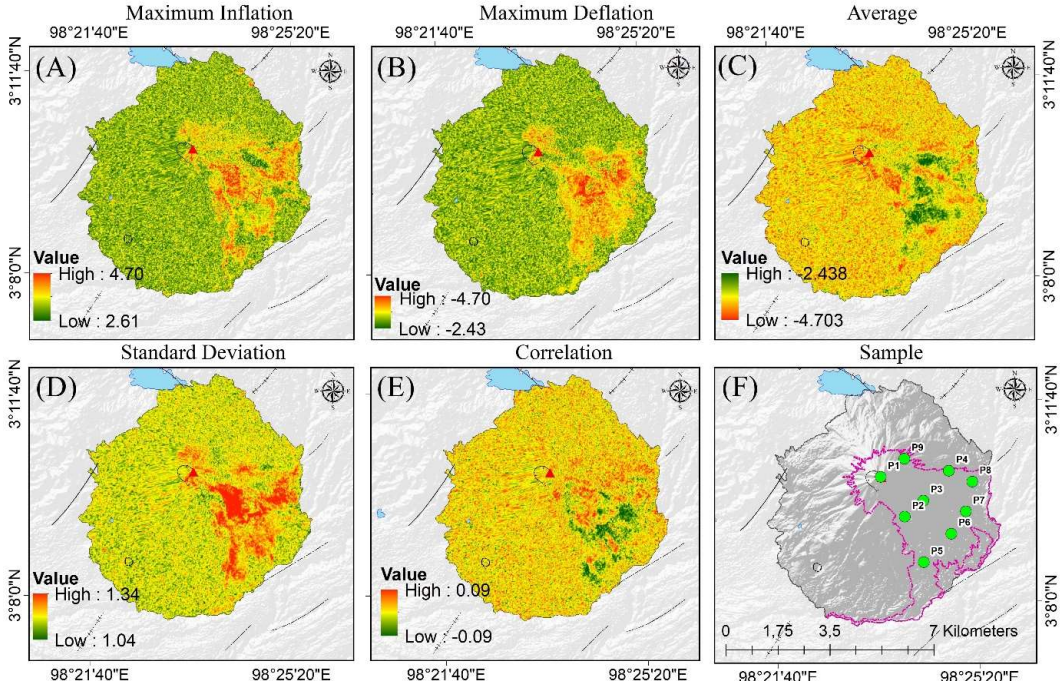

Figure 4 The report of the spatial statistical analysis of the monthly data deformation between 2017-2022 and the selected sample points with a high coherence.

This research placed its emphasis on the distinctive spatial patterns surrounding Mount Sinabung, which compared to the surrounding areas, exhibited stark differences. Figure 4 aids in identifying these patterns. The multi-temporal InSAR analysis results showed that there had been observable positive and negative correlations between deformation and the frequency of eruptions. The correlation values indicated a relatively weak relationship between deformation and the number of monthly eruptions over the span of six years (in the range of -0.09 and 0.09). Notably, the southeastern foothill zone stood out given that it had shown high levels of maximum inflation and deflation, a low correlation with the number of eruptions, and substantial variance in data over the six-year period.

In the field of volcano monitoring, the interpretation of remote sensing data plays a pivotal role in providing vital information about a volcano's activity. The fact that the deformation zone within the area of erupted material was more pronounced than in other regions is noteworthy. In this study, nine sample points designated with the code "P" were carefully selected from multiple locations with high coherence values that had exceeded the

established threshold. (See Figure 4(F).) These "P" sample points were distributed in areas composed of former eruptive material from Mount Sinabung. Please refer to Figure 5, which illustrates the variations in vertical deformation that were observed over the six-year period.

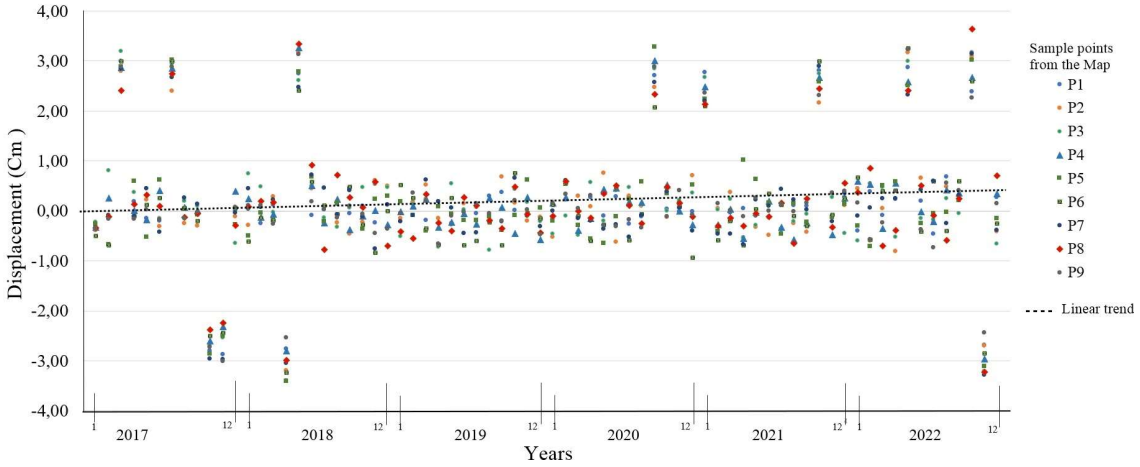

Figure 5 The annual deformation trend from 9 sample points of Sinabung Volcano from 2017 to 2022.

The results of the displacement data extraction for all "P" deformation samples over the six -year period revealed significant changes during several observation periods. In March, July, and October, inflation reached 3.6 cm, while in November of 2017, there was deflation of -3 cm. However, in 2018, a different pattern emerged, with deflation reaching -3.3 cm in April and inflation reaching 3.3 cm in May, which was followed by a return to the range of 1 to -1 cm. In September of 2020, and in January and October 2021, as well as in May and October of 2022, there was pronounced inflation that ranged from 2.0 cm to 3.9 cm at all observation points. However, in November of 2022, there was an exceptionally severe deflation event, with displacement values ranging from -2.0 to -3.0 cm. The highest average ground inflation rate was observed at the sample point of P3 at 1.73 cm/year. Meanwhile, the lowest rate of 0.62 cm/year was found at P6, where this sample point is located at the foot of the volcano.

The deformation zone surrounding Mount Sinabung strongly suggests that the magma system and underground reservoir remain active and play a significant role in shaping Mount Sinabung's deformation. The increase in both inflation and deflation, which surpassed the typical positive deformation trend within the observation range of -0.1 to 1.0 cm, is a clear indicator of this activity. Despite the absence of an explosive eruption, this deformation persists continuously, and the extreme fluctuations observed in the deformation data strongly imply that magmatic and volcanic processes continue to actively operate beneath the surface. Kobayashi's research [19] on volcanoes and hydrothermal systems underscores that magmatic activity can trigger anomalies in shallow hydrothermal systems. This, in turn, can induce deformation of the volcano's surface and elevate the fluid pressure within the rock, potentially resulting in the collapse of fractures and phreatic/phreatomagmatic eruptions, that can cause the area to become sensitive to earthquakes and dynamic magma pressure [20]. As an example, the 9.0 MW Aceh regional tectonic earthquake was positively associated with volcanic activity and the eruption of Mount Sinabung in 2010. Stress changes resulting from deformation, which is referred to as Coulomb stress, exhibit a positive correlation with shallow earthquakes that often originate in proximity to Mount Sinabung [21,22]. Therefore, it is important to note that volcanic deformation does not solely imply an imminent geohazard disaster like a volcanic eruption. Instead, it can also signify various aspects of volcanic activity, such as the potential for caldera collapse, landslides, or abnormal pressure changes within the hydrothermal system beneath the volcano.

The deformation dynamics uncovered in this study align with the findings from previous research that had been conducted on Mount Sinabung. The highly fluctuating pattern of inflation and deflation is not uncommon when monitoring volcanic activity, since this deformation is connected to various processes taking place within both the volcano's internal and external systems. The outcomes of this research closely corresponded with the discoveries made by previous researchers, such as Kriswati et. al. [2] and Hendra et. al. [21], who noted that Mount Sinabung is situated in the vicinity of the regional Semangko fault and as such, exhibits local faults on its slopes [20]. Mount Sinabung's magmatic system possesses properties that make it sensitive to stress changes. Even minor stress variations can trigger volcanic activity. Moreover, alterations in stress, coupled with reduced pressure, can readily induce magma ascent and other seismic events, as exemplified by the 2013 eruption. The notable local seismic activity on Mount Sinabung, which experienced positive Coulomb stress changes due to deformation, signifies that substantial pressure still remains stored within the Earth's crust [6,8]. Mount Sinabung's

extreme sensitivity to stress changes can readily trigger various geohazard disasters, including eruptions, landslides, and collapses [20]. As previous research has demonstrated, deformation changes resulting from tectonic earthquakes play a significant role in influencing Mount Sinabung's deformation conditions and its potential for eruption. Therefore, the continuous monitoring of volcanic deformation and the application of advanced geospatial methods are paramount for the surveillance of the Sinabung Volcano. This is especially relevant given the observation of random spatially distributed deformations, as well as periods of maximum inflation and deflation that do not necessarily correspond to the number of eruptions. Additionally, when assessing geological hazards for volcanic disaster management, the connection of Mount Sinabung to its geological environment renders the mountain highly sensitive to tectonic activities. The government and stakeholders are advised to closely monitor Mount Sinabung's activity, as it provides early warnings to the community and helps in decision-making and regional planning around the mountain. This is crucial in the context of mitigating future volcanic disasters.

4. Conclusion

This research has provided valuable insights into the monthly deformation activities of the Sinabung Volcano. The coherence value is one reference for the interferometry results. Less than 30% of the area of Mount Sinabung is covered by the zone with an InSAR phase coherence of more than 0.35 throughout the 6-year period. The occurrences of extreme inflation and deflation suggested that the land surface had undergone relatively significant changes in elevation. In some periods, inflation and deflation exceeded the average deformation values, while the correlation between the number of monthly eruptions and deformation was very weak. This implies that there is not a strong relationship between the frequency of eruptions and deformation. This observation is further supported by the monthly deformation data, in which inflation and deflation fluctuations were detected even in the absence of volcanic eruptions. Consequently, this deformation does not follow any constant or periodic patterns. The extreme fluctuations in deformation within this region are evident based upon the diverse deformation data with high data distribution and variance values. Random changes were observed in several volcanic areas. For instance, observations within the mountain caldera indicated a deformation trend, which was characterized by an increase in the surface elevation of Mount Sinabung. Despite the absence of explosive eruptions, the mountain's caldera continues to undergo growth and changes. Regarding future works, it is imperative to thoroughly examine the ground deformation fluctuations by considering the supplementary variables that can affect surface deformation, such as precipitation, slope characteristics, geological factors, temperature, geochemistry, and frequency of the earth's movement, as well as predict future eruptions.

5. Acknowledgements

The authors sincerely thank the College of Computing, Khon Kaen University, for providing a full scholarship (Announcement No. 646/2022) to complete this study. We also thank the College's Master's program in Geoinformatics for providing tools, facilities, and full support throughout the educational process.

6. Conflicts of interest

The authors confirm that there are no known conflicts of interest associated with this publication and there has been no significant financial support for this work that could have influenced its outcome.

7. References

[1] Pallister J, Wessels R, Griswold J, McCausland W, Kartadinata N, Gunawan H, Budianto A, Primulyana S. Monitoring, forecasting collapse events, and mapping pyroclastic deposits at Sinabung volcano with satellite imagery. J Volcanol Geotherm Res. 2019;382(3):149-163.

[2] Kriswati E, Meilano I, Iguschi M, Abidin HZ, Surono. An evaluation of the possibility of tectonic triggering of the Sinabung eruption. J Volcanol Geotherm Res. 2019;382(4):224-232.

[3] Seropian G, Kennedy MB, Walter RT, Ichihara M, Jolly AD. A review framework of how earthquakes trigger volcanic eruptions. Nat Commun. 2021;12(1):1-13.

[4] Nurwihastuti WD, Astuti DJ, Yuniastuti E, Perangin-angin R, Simanungkalit MN. Volcanic hazard analysis of Sinabung volcano eruption in Karo, North Sumatra, Indonesia. IOP Conf Ser: J Phys: Conf Ser. 2019;1175(1):012186.

[5] Mulyaningsih, Sri. Vulkanologi. Jl Progo B-15. Yogyakarta: Publisher Ombak Press; 2015.

[6] Corsa B, Barbara-Selvilla M, Tiampo K, Meertens C. Integration of DInSAR Time Series and GNSS Data for Continuous Volcanic Deformation Monitoring and Eruption Early Warning Applications. Remote Sens. 2022;14(3):2-24.

[7] Hanif M, Apichontrakul S. Vertical ground deformation monitoring of the sinabung volcano in 2021-2022 using sentinel-1 and DInSAR. Proceedings 12th International Conference on Environmental Engineering, Science, and Management. Jomtien Palm Beach Hotel & Resort, Pattaya, Thailand. May 17-18, 2023. p. 304-311.

[8] Saepuloh A, Wikantika K, Urai M. Observing lava dome roughness on synthetic aperture radar (SAR) data: Case study at Mt. Sinabung and Merapi - Indonesia. In: 2015 IEEE 5th Asia-Pacific Conference on Synthetic Aperture Radar (APSAR). IEEE; 2015.

[9] Lee WC, Lu Z, Kim WJ. Monitoring mount Sinabung in Indonesia using Multi-Temporal InSAR. Korean J Remote Sens. 2017;33(1):37-46.

[10] Aditya A, Aoki Y, Anugrah DR. Surface deformation monitoring of Sinabung volcano using multi-temporal InSAR method and GIS analysis for affected area assessment. IOP Conf Ser Mater Sci Eng. 2018;344(3):1-10.

[11] Razi P, Sri Sumantyo JT, Perissin D, Putra A, Hamdi, Widodo J, et al. Ground deformation measurement of Sinabung vulcano eruption using DInSAR technique. J Phys Conf Ser. 2019;1185:012008.

[12] Kim JR, Cheng-Wei L, Shih-Yuan L. The use of InSAR phase coherence analyses for the monitoring of aeolian erosion. Remote Sens. 2021;13(12):1-24

[13] Ullo LS, Pia A, Sica S, Martier D, Fiscante N, Cicala L. Application of DInSAR technique to high coherence Sentinel-1 images for dam monitoring and result validation through in situ measurements. IEEE J Sel Top Appl Earth Obs Remote Sens. 2019;12(3):875-890.

[14] Molan Es, Yusuf, Zhong L. Can InSAR coherence and closure phase be used to estimate soil moisture changes. Remote Sens. 2020;12(9):1-13.

[15] Cressie N, Moores MT. Spatial statistics. In: Sagar BS, Cheng Q, McKinley J, Agterberg F, editors. Encyclopedia of Earth Sciences Series. Cham: Springer International Publishing; 2023. p. 1–11.

[16] Scott LM, Janikas MV. Spatial statistics in ArcGIS. In: Fischer M, Getis A, editors. Handbook of Applied Spatial Analysis. Berlin, Heidelberg: Springer; 2010. p. 27-41.

[17] Romero-Puig N, Lopez-Sanchez M. A review of crop height retrieval using InSAR strategies: Techniques and challenges. IEEE J Sel Top Appl Earth Obs Remote Sens. 2021;14:7911-7930.

[18] Sica F, Scarpa G. A CNN-Based coherence-driven approach for InSAR phase unwrapping. IEEE Geosci Remote Sens Lett. 2022;19:1-5.

[19] Kobayashi T, Morishita Y, Munekane H. First detection of precursory ground inflation of a small phreatic eruption by InSAR. Earth Planet Sci Lett. 2018;491:244-254.

[20] Heap M, Tobias BH, Albert G, Stephan K, Amy R. Hydrothermal alteration can result in pore pressurization and volcano instability. Geology. 2021;49(11):1348-1352.

[21] Hendra Gn, Surono, Agus B, Kristianto, Oktory P, Wendy Mc, John P, Masato I. Overview of the eruptions of Sinabung Volcano, 2010 and 2013–present, and details of the 2013 phreatomagmatic phase. J Volcanol Geotherm Res. 2019;382:103-119.

[22] Parker AL, Biggs J, Walters JR, Ebmeier KS, Wright JT, Teanby AN, Lu Z. Systematic assessment of atmospheric uncertainties for InSAR data at volcanic arcs using large-scale atmospheric models: Application to the Cascade volcanoes, United States. J Remote Sens Environ. 2015;170:102-114.